

Article

Colorimetric Sensing of Benzoyl Peroxide Based on the Emission Wavelength-Shift of CsPbBr₃ Perovskite Nanocrystals

Li Zhang^{1,†}, Yimeng Zhu^{2,†}, Feiming Li², Linchun Zhang², Longjie You³, Zhiyong Guo¹, Yaning Huang⁴ ,
Li Zhao¹ and Xi Chen^{2,*} 

¹ Institute of Analytical Technology and Smart Instruments, College of Environment and Public Health, Xiamen Huaxia University, Xiamen 361024, China; zhangl@hxxy.edu.cn (L.Z.); guozhy@hxxy.edu.cn (Z.G.); zl@hxxy.edu.cn (L.Z.)

² State Key Laboratory of Marine Environmental Science, Xiamen University, Xiamen 361005, China; zhuym@xmu.edu.cn (Y.Z.); lfm1914@mnnu.edu.cn (F.L.); 20520191151446@stu.xmu.edu.cn (L.Z.)

³ National Quality Supervision and Inspection Center for Incense Products, Yongchun 362600, China; ycyj520@qzyczjs.com

⁴ Information Center, Xiamen Huaxia University, Xiamen 361024, China; hyn@hxxy.edu.cn

* Correspondence: xichen@xmu.edu.cn; Tel.: +86-592-2184530

† These authors contributed equally to this work.

Abstract: Using the ionic salt characteristics of CsPbBr₃ perovskite nanocrystals (CsPbBr₃ NCs), the fluorescence wavelength of CsPbBr_{3-x}I_x NCs could be changed by the halogen exchange reaction between CsPbBr₃ NCs and oleylammonium iodide (OLAM-I). Under the excitation of a 365 nm UV lamp and the increase of OLAM-I concentration, the content of iodine in CsPbBr_{3-x}I_x NCs increased, and the fluorescence emission wavelength showed a redshift from 511.6 nm to 593.4 nm, resulting in the fluorescence color change of CsPbBr₃ NCs from green to orange-red. Since OLAM-I is a mild reducing agent and easily oxidized by benzoyl peroxide (BPO), a novel colorimetric sensing approach for BPO based on the fluorescence wavelength shift was established in this study. The linear relationship between the different wavelength shifts ($\Delta\lambda$) and the concentration of BPO (C_{BPO}) is found to be in the range of 0 to 120 $\mu\text{mol L}^{-1}$. The coefficient of alteration (R^2) and the detection limit are 0.9933 and 0.13 $\mu\text{mol L}^{-1}$ BPO, respectively. With this approach, the determination procedure of BPO in flour and noodle samples can be achieved in only a few minutes and exhibit high sensitivity and selectivity.

Keywords: benzoyl peroxide; CsPbBr₃ nanocrystals; fluorescence wavelength shift; colorimetric sensing; halide exchange



Citation: Zhang, L.; Zhu, Y.; Li, F.; Zhang, L.; You, L.; Guo, Z.; Huang, Y.; Zhao, L.; Chen, X. Colorimetric Sensing of Benzoyl Peroxide Based on the Emission Wavelength-Shift of CsPbBr₃ Perovskite Nanocrystals. *Chemosensors* **2021**, *9*, 319. <https://doi.org/10.3390/chemosensors9110319>

Academic Editor: Philip Gardiner

Received: 11 October 2021

Accepted: 11 November 2021

Published: 14 November 2021

Publisher's Note: MDPI stays neutral with regard to jurisdictional claims in published maps and institutional affiliations.



Copyright: © 2021 by the authors. Licensee MDPI, Basel, Switzerland. This article is an open access article distributed under the terms and conditions of the Creative Commons Attribution (CC BY) license (<https://creativecommons.org/licenses/by/4.0/>).

1. Introduction

In halide perovskite ABX₃, X is the halogen anion (Cl⁻, Br⁻, or I⁻), A is the monovalent cation Cs⁺ CH₃NH₃⁺ (MA) or CH(NH₂)₂⁺ (FA), and B is a divalent metallic cation, such as Pb²⁺, Sn²⁺, or Ge²⁺. Although the discovery of halogen perovskites can be traced back to 1958 [1], they did not attract much attention until the study of Miyasaka et al. using MAPbI₃ for solar cells in 2009; the research upsurge of lead halide perovskites (LHPs) attracted wide attention in relevant fields [2]. The photogenerated electrons and holes of LHPs can not only be separated to produce an electric current, but can also be combined to produce light through radiation. LHPs have the characteristics of narrow emission peak, high color purity, and accurate adjustment of emission wavelength through halogen composition in the whole visible region, which indicates application potential in lighting [3–5], optical display [6–8], laser [9,10], and optical sensing and detection [11–13]. However, the fluorescence quantum yield (PLQY) of the macro-sized LHPs is generally not very high, since (a) LHPs have a low generation energy of ion defects (especially halogen defects) and are prone to produce a large number of ion vacancy defects during crystallization; and (b)

LHPs have low exciton binding energy, resulting in low electron-hole radiative recombination efficiency. Therefore, researchers have turned their attention to lead halide perovskite nanocrystals (CsPbBr₃ NCs), in an attempt to improve the exciton binding energy and radiation recombination efficiency of LHPs by enhancing the quantum confined effect [14]. In 2014, Perez-Prieto et al. first reported the synthesis of MAPbBr₃ NCs, whose PLQY could be closer to 20% [15]. In 2015, Kovalenko et al. synthesized and obtained 90% all-inorganic CsPbX₃ NCs for the first time [16], which started the vigorous development of CsPbBr₃ NCs in the field of luminescence. As shown in Figure 1, the halogen exchange characteristics of CsPbX₃ NCs cause the wavelength shift of their fluorescence emission [17]. Generally, the redshift of fluorescence wavelength occurs with the increase of X ion radius. For example, iodide can exchange Br in CsPbBr₃ PNCs, and result in the corresponding generation of CsPbBr_xI_{3-x} (0 ≤ x ≤ 3). The fluorescence emission wavelength of CsPbBr_xI_{3-x} gradually redshifts with the increase of iodine concentration, and the apparent color changes from green to red. The wavelength change has a linear relationship with the concentration of I⁻, which is very useful in colorimetric sensing for an oxidative substance due to the reduction property of iodide (I₂ + 2e⁻ → 2I⁻, with E^o -0.54 V vs. SHE).

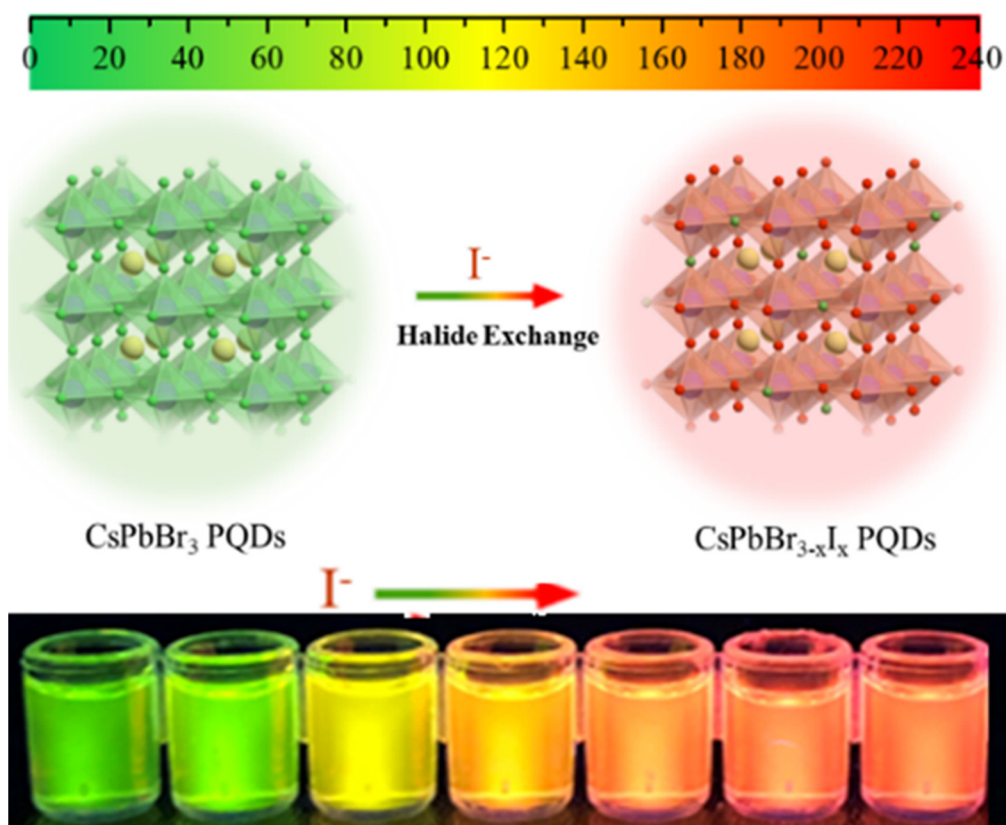


Figure 1. Schematic illustration of the fluorescent color based on the ion exchange of CsPbBr₃ PNCs induced by iodide (left side) and the appearing colors.

CsPbBr₃ NCs reveal their anion exchange within tens of seconds due to the ionic salt characteristics in which I⁻ or Cl⁻ ions produce CsPbBr_xI_{3-x} NCs and CsPbCl_xBr_{3-x} NCs after the exchange with CsPbBr₃ NCs is completed [17]. After the halogen exchange, the fluorescence emission wavelength of the CsPbBr₃ NCs will shift significantly and result in the obvious change of the emission color, which is conducive to colorimetric sensing. In addition to halogen exchange, cations in CsPbBr₃ NCs can also be exchanged; for example, in the presence of Hg²⁺, Pb²⁺ in CsPbBr₃ NCs could gradually be replaced by Hg²⁺ [18]. The different fluorescence responses of MAPbBr₃ NCs could be obtained if their crystal structure changes. A typical example is the generation of MAPbBr₃•H₂O by MAPbBr₃ NCs and water molecules in a certain humidity range [19]. CsPbBr₃ NCs are one of many

superficial defects, and fluorescence sensing methods can be established by passivation of these superficial defects. For example, O₂ can significantly enhance the fluorescence of CsPbBr₃ nanosheets, CsPbBr₃ nanowires, and CsPbBr₃ single crystals due to their many surface defect states [20] which can be used for O₂ sensing. Common energy transfer in fluorescence sensing also is applied by using CsPbBr₃ NCs. Fluorescence resonance energy transfer is formed between CsPbBr₃ NCs/PS FM and Rhodamine 6G (Rh 6G), and thus a highly sensitive sensing method for Rh 6G was established [21]. By doping Mn²⁺ into CsPbBr₃ NCs, the O₂ sensing can be realized with good responses [22].

Colorimetric sensing has been applied in chemical analysis for its simplicity, rapid and direct readout analysis, lack of large complicated scientific instruments, and ability to achieve real-time and in-situ analysis. Ordinarily, the naked eye is insufficient in the resolving of intensity change in homochromatism (ca. 64 grades), but it has a high sensitivity in the identification of color change (ca. 10 million color types). Recently, as shown in Table S1, there have been several reports on the studies and applications of colorimetric sensing based on the wavelength-shift of the halogen exchange characteristics of CsPbX₃ NCs. Chen et al. developed a novel colorimetric sensing approach for the peroxide number determination of edible oil, in which the edible oil sample underwent redox reactions with OLAM-I, and then a halogen exchange occurred between the added CsPbBr₃ NCs and the iodide ions from the residual OLAM-I [11]. A colorimetric sensing approach for the determination of Cl⁻ in sweat by the heterogeneous halide exchange between CsPbBr₃ NCs in n-hexane and Cl⁻ in an aqueous solution has also been presented [23]. Additionally, a sensing approach for methylamine (MA) gas has been set up with the fluorescence turn-on and wavelength shift in the formation of MAPbBr₃ NPs in hollow SiO₂ nanospheres triggered by the reaction between MA gas and HPbBr₃/PbBr₂@SiO₂ nanospheres [24]. In 2019, Lin et al. designed a simple device for the separation and sensing of H₂S with high sensitivity and selectivity using CsPbBr₃ NCs [20]. The fluorescence intensity was linearly related to H₂S concentration (in the range of 0~100 μM), and the detection limit was 0.18 μM. This approach was used to detect H₂S in rat brain microdialysis. In 2020, Yun et al. [25] synthesized a CsPbBr₃ PQDs/cellulose composite material and used it as an effective colorimetric sensing material for the real-time monitoring of chlorine, iodine, and other trace elements in tap water. The results showed an excellent sensitivity for the detection of iodide ions in the range of 0.0001 to 1 M, and the detection limit (LOD) was 2.56 mM. Similarly, the detection limit for chloride ions was 4.11 mM. Additionally, in 2021, the Jacek group [26] reported the sensing results for methane using the halogen exchange characteristics of CsPbX₃ NCs.

Flour is one of the most important foods in our diet. Generally, its color presents slightly yellow due to carotenoids, lutein, and other naturally colored nutrients. To improve the flour color, flour brightener, mainly containing benzoyl peroxide (BPO), has been used. BPO has strong oxidization characteristics and can improve the flour's apparent color, maturity period, and yield. However, due to the strong oxidation of BPO, the addition of BPO can damage the natural nutrients in flour. In addition, BPO causes a strong irritation to the skin and upper respiratory tract. An excess of BPO in the body will cause vertigo, vomiting, neurasthenia, and a variety of diseases, resulting in serious damage to the liver and other organs. Although the addition of BPO in the production process of all kinds of flour is prohibited [27], the illegal addition is still occasionally found due to its low cost and obvious bleaching effect.

As shown in Table S2, there have been a variety of determination methods for BPO such as gas chromatography (GC) [28], high-performance liquid chromatography (HPLC) [29–31], capillary electrophoresis (CE) [32], the electrochemical method [33,34], chemiluminescence [35,36], and the other optical methods [37–41]. To discover the presence of BPO easily and quickly, further efforts are necessary to develop real-time methods, including colorimetric determination. In this study, the halogen exchange reaction between CsPbBr₃ NCs and the iodine in oleylammonium iodide (OLAM-I) was studied. The relationship between the concentration of iodine in the solution and the fluorescence

wavelength shift has been observed and investigated. Using the redox reaction of BPO and iodine, we have developed a colorimetric sensing method based on the wavelength-shift for BPO using CsPbBr₃ NCs and applied the convenient and low-cost approach towards the determination of BPO in flour and noodle samples.

2. Materials and Methods

2.1. Materials and Chemicals

Cs₂CO₃ (99.9%), PbBr₂ (99.99%), oleic acid (OA, 90%), octadecene (Octadecene, ODE, 90%), oleylamine (OAM, 80–90%), and benzoic peroxide (99.9%) were all purchased from Aladin Reagent Co., Ltd. (Shanghai, China). FeCl₃, MgSO₄, NaCl, Na₂S, CaCl₂, NaI, KCl, NaNO₃, NaNO₂, NaClO, Na₃PO₄•12H₂O, NaH₂PO₄, Na₂CO₃, NaHCO₃, and Zn(NO₃)₂•6H₂O were purchased from Sinoptic Chemical Reagents Co., Ltd. (Shanghai, China). All other reagents were at least analytical grade and without further purification. The water used throughout the experiments was from a water purification system (Millipore, Burlington, MA, USA).

2.2. Instruments

The absorption spectra were characterized by a Hitachi UV-Vis 2550 spectrophotometer. Fluorescence spectra of CsPbBr₃ NCs were collected by an F-4500 fluorescence spectrophotometer (Hitachi, Tokyo, Japan). The in-situ halogen exchange between Br and I was observed using a Renishaw Invita Raman (Renishaw, London, UK) spectrometer with a laser excitation source (457 nm). The morphology of CsPbBr₃ NCs was characterized by JEOL-1400 transmission electron microscopy (TEM, Tokyo, Japan), and the relevant acceleration voltage was set at 100 kV.

2.3. Preparation of Materials

2.3.1. Preparation of Cesium Oleate

In the preparation of cesium oleate [16], 0.814 g of CS₂CO₃, 40 mL of octadecene solution, and 2.5 mL of oleic acid were added and mixed into a 50 mL three-necked flask. The CS₂CO₃ was completely dissolved and reacted at 120 °C in a vacuum resulting in a brownish-yellow solution. This product was prepared for the subsequent experiments.

2.3.2. Preparation and Purification of CsPbBr₃ NCs

The CsPbBr₃ NCs were prepared per the report with some adaptations [16]. A preparation of 0.069 g of PbBr₂, 5 mL of octadecene solution, 0.6 mL of oleic acid, and 0.5 mL of oleic amine were added into a 25 mL three-necked flask. The flask was then placed under a vacuum and heated to 120 °C. The temperature was held constant until the PbBr₂ was completely dissolved, then the temperature was increased to 150 °C. A total of 0.4 mL of prepared product and cesium oleate, was quickly injected into the three-necked flask at 150 °C in a nitrogen environment. After the injection, the flask was quickly placed in an ice water bath and shaken continuously to obtain a yellow-green colloidal product, which was removed and kept at room temperature.

The yellow-green liquid of the obtained product was centrifuged at 10,000 rpm for 10 min. The bottom precipitates were then retained and the supernatant discarded. A total of 2 mL n-hexane was added to the precipitate to disperse the CsPbBr₃ NCs. The final product was stored in a refrigerator for subsequent experiments.

2.3.3. Synthesis of Oleylammonium Iodide

Oleylammonium iodide (OLAM-I) was prepared per the report [42]. In a nitrogen environment, 8 mL oleylamine and 3 g I₂ were added to a 50 mL three-neck flask with magnetic stirring at 2500 rpm. Then the flask was heated to 140 °C under nitrogen protection. When the solution became clear, the heating temperature was raised to 180 °C. A yellow-brown solution of OLAM-I was then obtained and stored in a nitrogen environment in a refrigerator for the subsequent experiments.

2.3.4. Fluorescence Wavelength-Shift with the Different OLAM-I Concentration

Different 2 mL concentrations (0 to 260 $\mu\text{mol L}^{-1}$) of the OLAM-I n-hexane solution were added to 5 mL centrifuge tubes followed by 50 μL CsPbBr₃ PNCs. After a 2 min reaction, their fluorescence spectra were measured. Meanwhile, their apparent colors under the excitation of a 365 nm UV lamp were collected by a camera.

2.3.5. BPO Concentration and the Corresponding Wavelength-Shift

Different 1 mL concentrations of a BPO (0–120 $\mu\text{mol L}^{-1}$) toluene solution were added into 5 mL centrifuge tubes followed by 2 mL of 240 $\mu\text{mol L}^{-1}$ OLAM-I and allowed to react for 5 min. Afterwards, 50 μL CsPbBr₃ PNCs were added for the fluorescence spectra measurement. The fluorescence wavelength of the solution with 0 $\mu\text{mol L}^{-1}$ BPO was taken as λ_0 , and those of different concentrations of BPO were λ_x . Their difference was considered as $\Delta\lambda = \lambda_0 - \lambda_x$. A relationship curve between the concentration of BPO and $\Delta\lambda$ was obtained, which was used as the standard working curve for BPO.

In the sample pre-preparation for the BPO determination of flour or noodle samples, the noodle samples were first ground, and then the noodle and flour samples were filtered through a 600-mesh filter. After filtering, 1,000 g of flour or noodle powder was added into a 10 mL centrifuge tube with 5 mL toluene then added. BPO in the sample was extracted using ultrasonic means for 30 min, and then the tube was centrifuged at 10,000 rpm for 10 min. The supernatant solution was used for the BPO determination as referred to in the above experimental procedures. Then 1 mL of supernatant solution from the sample was added into a 5 mL centrifuge tube containing 1 mL of 240 $\mu\text{mol L}^{-1}$ OLAM-I solution. The solution was shaken for 10 min, and then 50 μL CsPbBr₃ PNCs in n-hexane were added. Their fluorescence spectra were recorded after the solution was shaken for 1 min. The BPO concentration was then obtained based on the wavelength shift of the corresponding fluorescence emission.

3. Results and Discussion

3.1. Spectroscopy and Structural Characterization of CsPbBr₃ PNCs

Sensing reproducibility and accuracy are greatly dependent on the fluorescence characteristics of CsPbBr₃ PNCs and are affected by their size and uniformity. As shown in Figure 2b, the CsPbBr₃ PNCs are of uniform size with an average diameter of about 15 nm, and present promising fluorescence characteristics with the maximum emission at 515 nm with a 22 nm half peak width (Figure 2a), and 87% fluorescence quantum yield (PLQY).

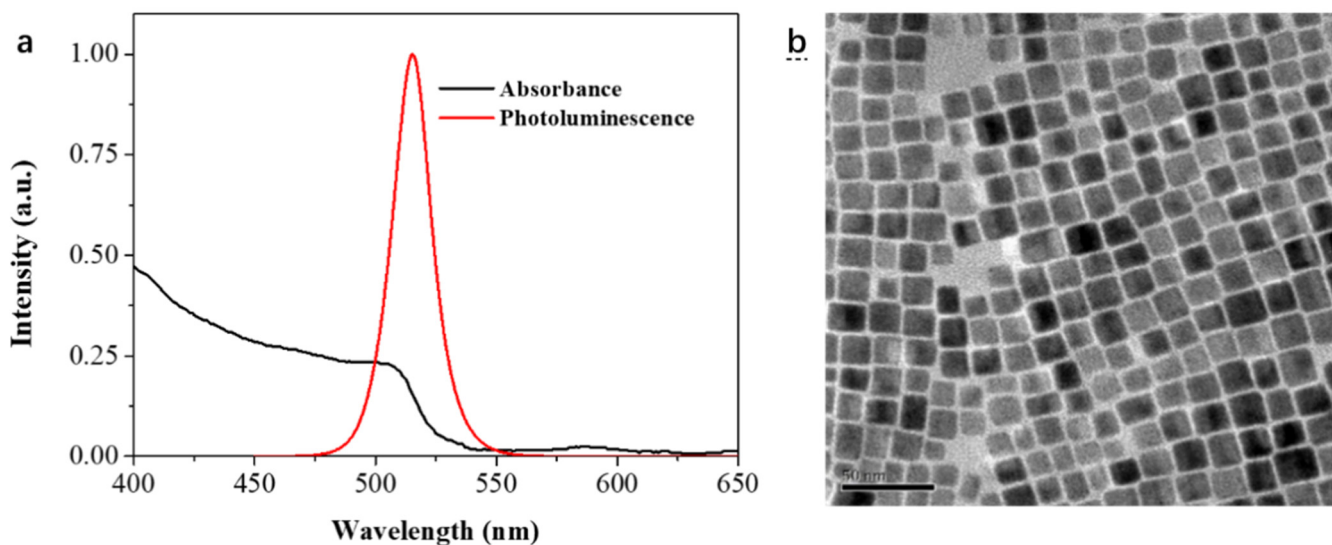


Figure 2. Absorbance and fluorescence spectra of the synthesized CsPbBr₃ PNCs (a) and their TEM images (b).

3.2. Fluorescence Wavelength-Shift in the Halogen Exchanges of CsPbBr₃ PNCs

In this study, the halogen exchange process of CsPbBr₃ PNCs with I[−] in homogeneous and heterogeneous phases was investigated. CsPbBr₃ PNCs and OLAM-I were selected for the study of the homogeneous halogen exchange. In this study, heterogeneous halogen exchange on a water/organic or a solid/liquid interface was considered. NaI aqueous solution and CsPbBr₃ PNCs in a n-hexane solution were focused on for the halogen exchange study of the water/organic phase, while NaI solid powder and CsPbBr₃ PNCs in n-hexane were used for the solid/liquid phase. Following the study of Kamat et al. [43], three steps occur in the halogen exchange between CsPbBr₃ PNCs in n-hexane and I[−] including: (1) diffusion of I[−] to the CsPbBr₃ PNCs interface; (2) interfacial halogen exchange; and (3) I[−] diffusion of CsPbBr₃ PNCs in crystals. In this experiment, to understand the halogen exchange process of CsPbBr₃ PNCs and I[−], a constant concentration of CsPbBr₃ PNCs was used to keep the characteristic absorption of CsPbBr₃ PNCs at 335 nm. In this study, the interfacial exchange between water and the organic phase is first considered. After a halogen exchange, the CsPbBr_xI_{3−x} PNCs become more unstable in a polar reagent such as ethyl acetate, so n-hexane was selected as the dispersion solvent of CsPbBr₃ PNCs in the experiment. Due to the great polarity differences between H₂O and n-hexane, it is difficult to effectively exchange I[−] in water to n-hexane. Generally, higher concentrations of NaI (60 mmol L^{−1}), acidic condition (pH 1), and a quick stir rate (1500 rpm, 5 min) are necessary to realize the exchange. As shown in Figure 3, the fluorescence emission wavelength of CsPbBr₃ PNCs shifted from 518 nm to 549 nm. However, in a neutral medium (pH 7), the whole exchange process became very slow, and it took more than 24 h to finish the reaction process.

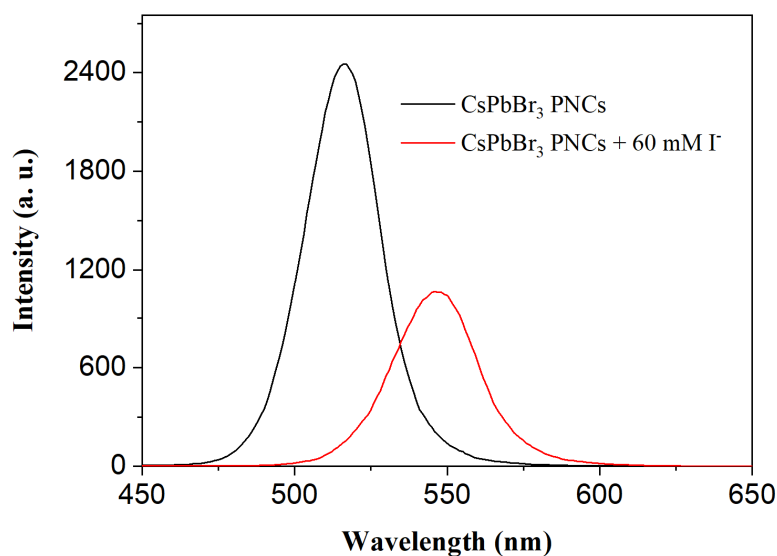


Figure 3. Fluorescence spectra of halide exchanges between CsPbBr₃ PNCs hexane and NaI aqueous solution (60 mmol L^{−1}).

The halogen exchange on the solid/liquid interface was also investigated. The process of in-situ halogen exchange between CsPbBr₃ PNCs in n-hexane and NaI powder was observed using a Renishaw Invita Raman spectrometer. The schematic diagram of the experiment was shown in Figure 4. As shown in Figure 5, each spectrum was collected at 30 s intervals. Analysis of the spectrum change indicated that the I[−] and Br[−] exchange occurred quickly on the NaI crystal interface as soon as the addition of CsPbBr₃ PNCs. The initial fluorescence emission at 518 nm of CsPbBr₃ PNCs changed to 625 nm due to the exchange between the NaI crystal interface and CsPbBr₃ PNCs. The wavelength at 625 nm should be relegated to the exchange product as CsPbBr_xI_{3−x} (CsPbBr_xI_{3−x} is the existing form on the solid/liquid interface, but CsPbBr_xI_{3−x} is the form after the exchange in the solution). When the exchange of CsPbBr_xI_{3−x} and NaI crystals in the solution was

carried out further, increasing the iodine content in the $\text{CsPbBr}_x\text{I}_{3-x}$, the fluorescence peak of $\text{CsPbBr}_x\text{I}_{3-x}$ was continuously redshifted in wavelength and its intensity enhanced. However, with the exchange time increased, the redshift rate of $\text{CsPbBr}_x\text{I}_{3-x}$ on the interface of NaI crystals was greatly reduced, due to the slow diffusion into the crystal interior. Finally, the fluorescence wavelength of the interface between the solution and NaI crystal overlaps, indicating that the exchange reached an equilibrium state in about 20 min.

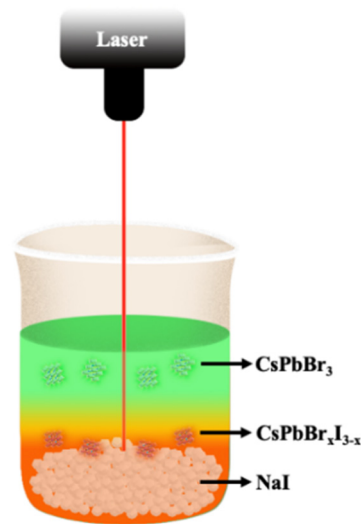


Figure 4. Experimental sketch for the halogen exchange on the solid/liquid interface.

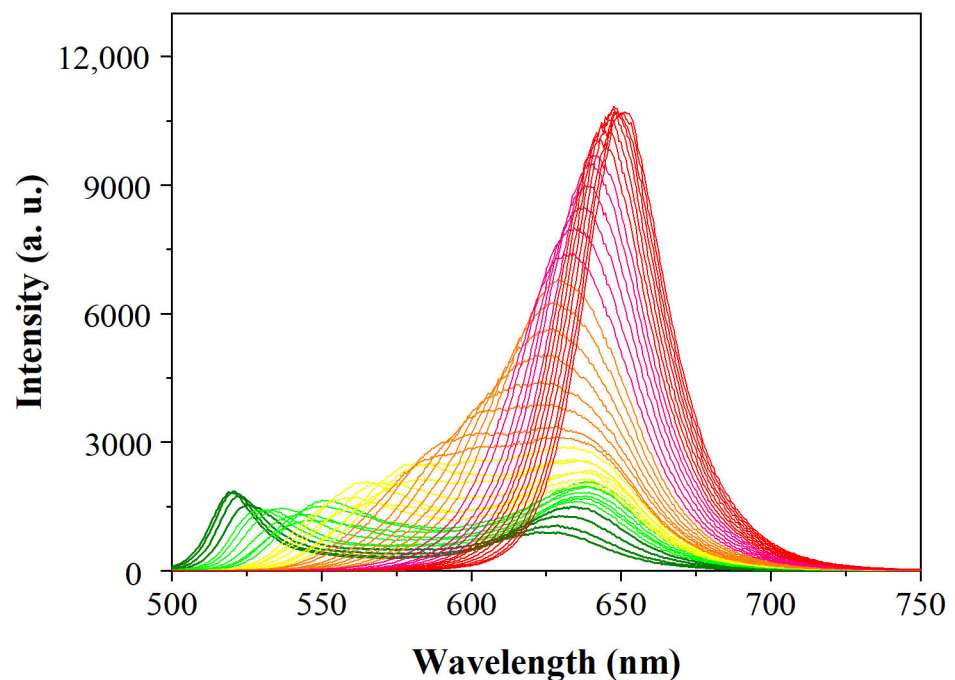


Figure 5. Fluorescence spectra of halide exchanges between CsPbBr_3 PNCs in n-hexane and NaI powder.

The halogen exchange between CsPbBr_3 PNCs and OLAM-I in n-hexane solution was further studied. The results as shown in Figure 6 indicated that OLAM-I presents good solubility in n-hexane. When different concentrations of OLAM-I were added to CsPbBr_3 PNCs in n-hexane, the halogen exchange could be carried out rapidly, revealing a single exponential process (Figure 6a). The exchange is essentially a surface-restricted exchange process and could generally be completed within 2 min ($\text{OLAM-I} = 120 \mu\text{mol L}^{-1}$). In

addition, it was found that the reaction was mainly controlled by the kinetic process, and that temperature had little effect on the halogen exchange in the range of 15 °C to 45 °C, which is convenient for the application at room temperature. The halogen exchange between the different concentrations of OLAM-I and CsPbBr₃ PNCs was further investigated. As shown in Figure 6b, the yellowish-green color of the n-hexane solution containing CsPbBr₃ PNCs changed to orange-red and red rapidly with the concentration increase of OLAM-I due to the generation of CsPbBr_xI_{3-x}. The bandgap width of CsPbBr_xI_{3-x} decreases with the increasing content of I, corresponding to the red-shift of the band-edge absorption and the emission spectrum. The corresponding color changed from green to yellow, and then red (Figure 6c). Experimental results reveal that the proposed method is of high resolution in colorimetric sensing, and the redshift of the wavelength difference ($\Delta\lambda$) and the concentration of OLAM-I presents a good linear relationship in the range of 0 to 240 $\mu\text{mol L}^{-1}$ (Figure 6d); the corresponding linear equation for $\Delta\lambda = 0.563 C_{\text{OAmI}}$ ($\mu\text{mol L}^{-1}$), $R^2 = 0.9960$.

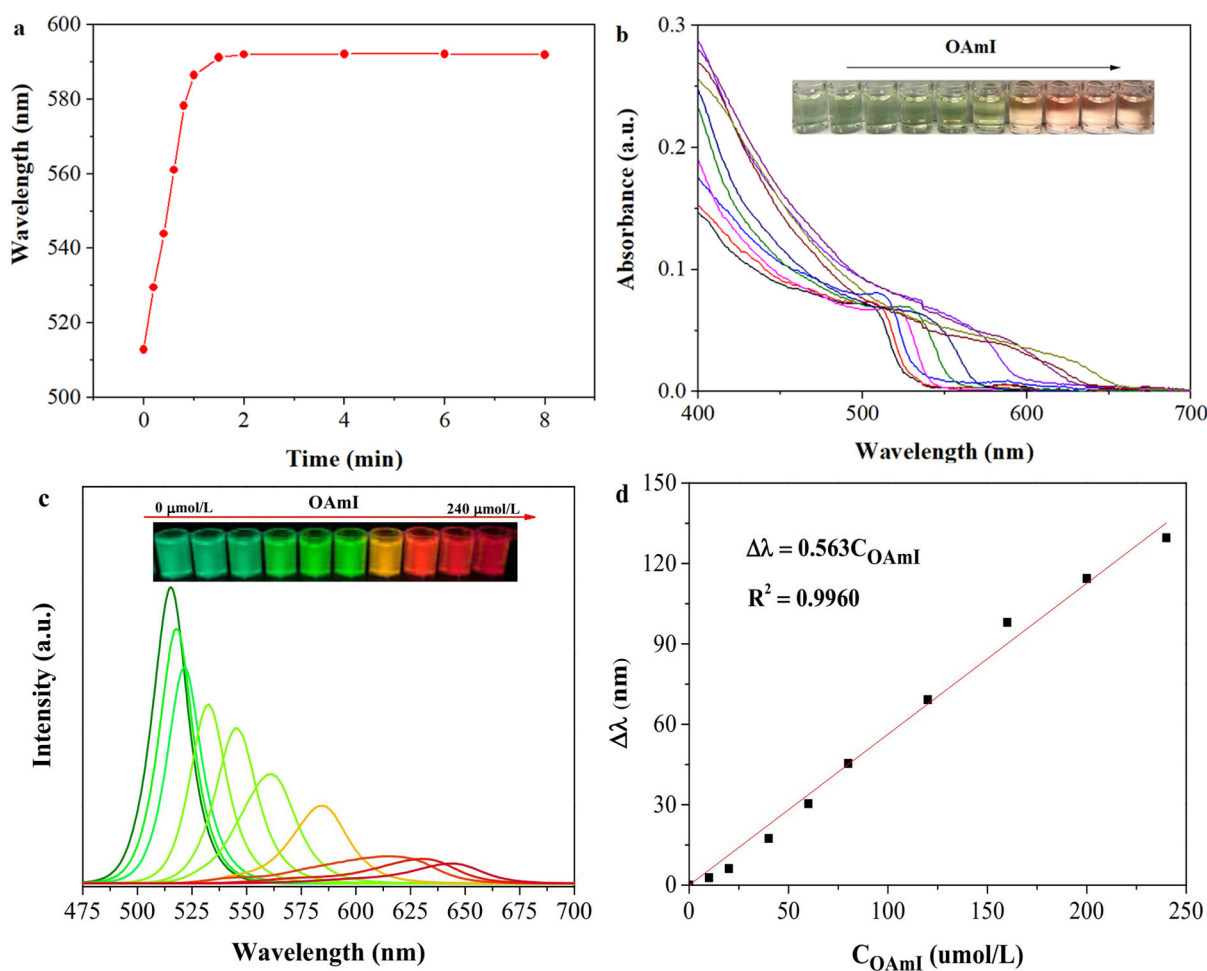


Figure 6. (a) The wavelength changes of CsPbBr₃ PNCs with halide exchanges of 120 $\mu\text{mol L}^{-1}$ OLAM-I at different times; (b,c) the band edge absorption and PL spectra changes when CsPbBr₃ PNCs halide exchange with OLAM-I of different concentration from 0–240 $\mu\text{mol L}^{-1}$; (d) the relationship between the concentration of OLAM-I and the wavelength-shift.

3.3. Analytical Performance of the Sensing Approach

Before the applications using the wavelength-shift-based sensing of the CsPbBr₃ PNCs for the determination of BPO, the validation method included linear range, the limit of detection (LOD), the limit of quantitation (LOQ), precision, and accuracy under optimized conditions. BPO has high oxidization characteristics and a good solubility in organic solvents. As shown in Figure 7a, BPO oxidizes OLAM-I, which reduced the halogen

exchange between iodine and CsPbBr₃ PNCs, resulting in the decrease of wavelength redshift in the reaction. The following experimental phenomena would verify the reaction process as 1 mL of 240 μmol L⁻¹ OLAM-I reacted with different concentrations of BPO (0~120 μmol L⁻¹ in toluene). After the reaction was complete, CsPbBr₃ PNCs in an n-hexane solution was then added to observe the halogen exchange. The results showed that BPO reacted completely with OLAM-I within 5 min and directly reduced the halogen exchange of CsPbBr₃ PNCs. In the absence of BPO, as shown in Figure 7b, the apparent color of CsPbBr₃ PNCs changed from the original green to the red of CsPbBr_xI_{3-x}. With the increase of BPO concentration, although the wavelength redshift of the fluorescence emission could be observed in the reaction of OLAM-I and CsPbBr₃ PNCs, the apparent color changed from red to orange, yellowish-green, and finally green, indicating the concentration decrease of OLAM-I due to the addition of BPO.

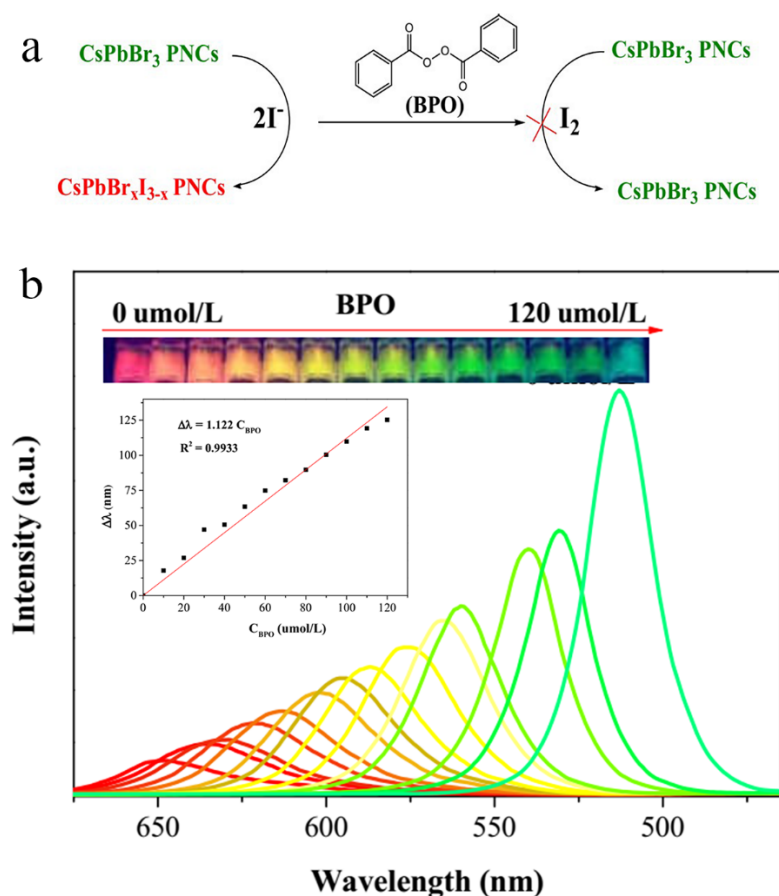


Figure 7. (a) Schematic mechanism illustration of wavelength shift-based fluorescence colorimetric sensing of BPO based on the CsPbBr₃ PNCs halide exchange caused by the oxidation reaction between OLAM-I and BPO; (b) Fluorescence spectrum changes when CsPbBr₃ PNCs halide exchange with 240 μmol L⁻¹ OLAM-I under the different concentrations of BPO from 0 to 120 μmol L⁻¹; inset, the linear relationship between the BPO concentration and the corresponding wavelength-shift ($\Delta\lambda$).

In the presence of 120 μmol L⁻¹ BPO, OLAM-I was completely oxidized, and no halogen exchange could be found for CsPbBr₃ PNCs. The experimental results as shown in the inset of Figure 8b reveal that 0~120 μmol L⁻¹ BPO could be detected with this method. When the concentration of BPO exceeded 120 μmol L⁻¹, the BPO would further oxidize CsPbBr₃ PNCs, resulting in poor stability and interference in the determination due to the strong oxidation characteristics of BPO. The wavelength shift difference, $\Delta\lambda$, presented a good linear relationship with the concentration of BPO (C_{BPO}) in the range of 0~120 μmol L⁻¹; the linear equation for $\Delta\lambda = 1.122 C_{\text{BPO}}$ ($R^2 = 0.9933$). Based on the limit of detection (LOD) = $3\sigma/K$ (where σ is the relative standard deviation of 12 blank

measurements and k is the slope of the linear equation), the LOD and LOQ of $0.13 \mu\text{mol L}^{-1}$ and $0.43 \mu\text{mol L}^{-1}$ BPO could be obtained, respectively. The experimental results revealed that the alteration of the intraday coefficient for five duplicate samples of $10 \mu\text{mol L}^{-1}$ BPO was less than 4.2%. Meanwhile, the alteration of the interday coefficient was less than 5.6% for the same concentration of BPO during three days.

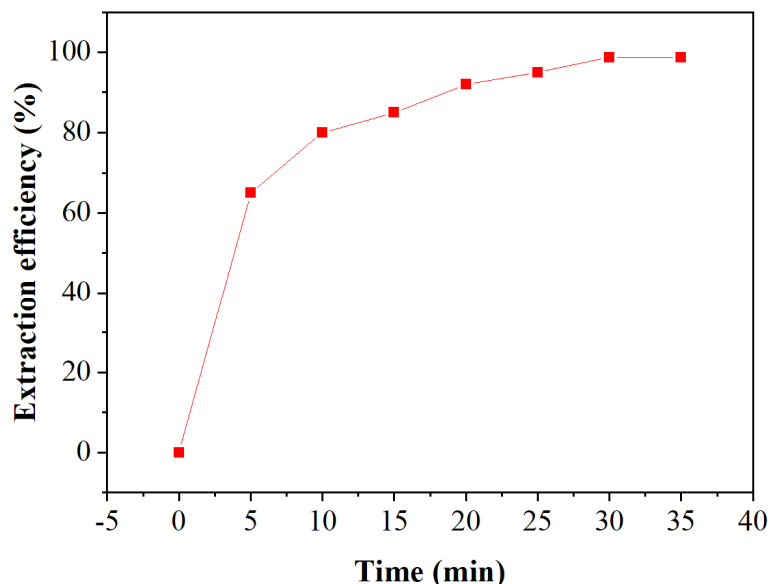


Figure 8. Extraction efficiency under different extraction times.

3.4. Determination of BPO in Samples

In the determination of BPO in flour and noodle samples, pretreatment is the key step. The BPO sample extraction procedures and timing were selected and optimized. Ultrasonic extraction was selected since the ultrasonic process is simple, highly efficient, and can effectively remove the dissolved oxygen in the solvent thus reducing the interference caused by the reaction of dissolved oxygen and OLAM-I. In the separation process, a direct filtration treatment method was applied in the National Standard Method (GB/T 18415-2001 Determination of Benzoyl Peroxide in Wheat Flour). However, flour particles easily block the pores of filter paper, which leads to problems such as irregular filtration, loss of extract, and incomplete extraction. In addition, the volatilization of organic extract in the filtration process can cause deviation of the test results and environmental pollution. In the experiment, the centrifugal precipitation separation method was adopted to achieve higher separation efficiency, more thorough extraction, and a smaller impact on the determination results. At the same time, using the centrifugal separation method significantly reduces the harm to the experimenter and the environmental pollution. The ultrasonic time was optimized as such: 1 g of flour or noodle powder was collected (BPO was added to the flour to make the mass concentration of BPO 24.2 mg kg^{-1}), and 5 mL of n-hexane was used for the extraction. Generally, with the increase of extraction time, the extraction yield of BPO increased continuously, and so the concentration of BPO would be $120 \mu\text{mol}\cdot\text{L}^{-1}$ if the extraction efficiency was 100%. Based on the redshift of the fluorescence emission wavelength, the experimental results as shown in Figure 8, indicate that 99.7% BPO in the sample could be extracted after 30 min. Thus, the optimal extraction time of 30 min was selected.

The effect of possible co-existing substances' influence on the sensing was investigated, and the results are shown in Figure 9. The experimental results show that the influence of common cations on the sensing determination was very small, revealing the selection of n-hexane as an ideal extracting solvent for BPO. BPO can be dissolved in n-hexane, while other co-existing substances (such as KI, MgSO_4 , etc.) had poor solubility in n-hexane, which reduces their possible effect, and thus greatly improves the selectivity. The influence

of sample humidity on the results was also studied. In the test environment with a humidity of 75%, the samples were allowed to fully absorb water in the air for one night. At the same time, another flour or noodle sample was dried using a vacuum to compare the sensing response with those samples in 75% humidity. The results indicated that there was no significant difference between the two conditions. This indicates that the water adsorption in the samples did not affect the sensing results because it is very difficult to dissolve the high polarity molecule, H₂O, into n-hexane, resulting in the insignificant effect of humidity on the sensing results.

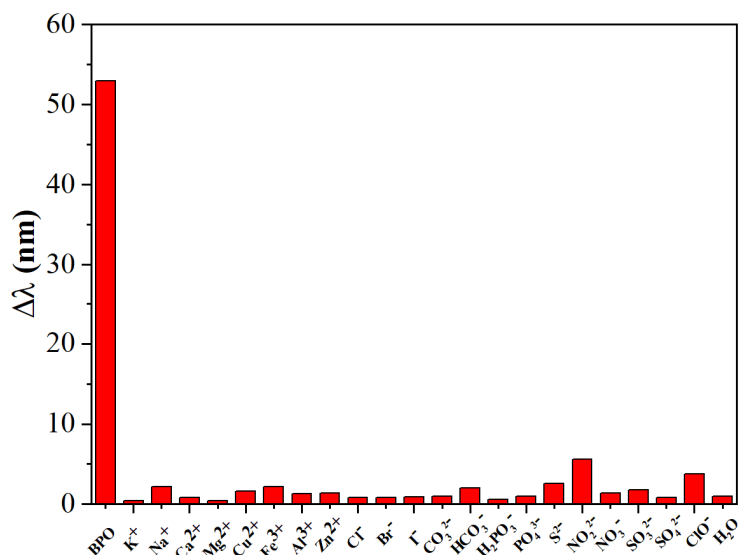


Figure 9. Sensing selectivity in the BPO determination. The mass concentration of the coexistence compounds from left to right were: 0.7 mg kg⁻¹ BPO, 5.3 g kg⁻¹ KCl, 5.3 g kg⁻¹ CaCl₂, 10.0 g kg⁻¹ NaCl, 7.2 g kg⁻¹ MgSO₄, 7.2 g kg⁻¹ MgSO₄ CuCl₂, 7.2 g kg⁻¹ MgSO₄ FeCl₃, 7.2 g kg⁻¹ AlCl₃, 5.3 g kg⁻¹ KBr, 7.6 g kg⁻¹ NaI, 5.5 g kg⁻¹ Na₂CO₃, 8.3 g kg⁻¹ NaHCO₃, 7.6 g kg⁻¹ Na₃PO₄•12H₂O, 7.6 g kg⁻¹ NaH₂PO₄, 5.6 g kg⁻¹ Na₂S, 5.0 g kg⁻¹ NaNO₂, 5.6 g kg⁻¹ Zn(NO₃)₂•6H₂O, 5.0 g kg⁻¹ Na₂SO₃, 0.7 mg kg⁻¹ NaClO, and humidity absorbed H₂O on flour.

Using the above optimal conditions, the colorimetric sensing of BPO in flour and noodle samples was carried out. As shown in Table 1, the sensing results of the recovery ranged from 97.0% to 112.0%, indicating that the method has good accuracy and application potential.

Table 1. Sensing results for BPO in flour and noodle samples.

Sample	BPO (μmol L ⁻¹)	Spiked (μmol L ⁻¹)	Found (μmol L ⁻¹)	RSD (%; n = 6)	Recovery (%)
Flour 1	ND	5.0	5.2 ± 0.2	3.8	104.0
		10.0	10.6 ± 0.5	4.7	106.0
		5.0	5.4 ± 0.2	4.0	108.0
Flour 2	ND	10.0	11.2 ± 0.4	3.5	112.0
		5.0	5.5 ± 0.3	5.5	110.0
Flour 3	ND	10.0	10.2 ± 0.4	4.2	102.0
		5.0	4.9 ± 0.2	4.3	98.0
Noodle 1	ND	10.0	9.8 ± 0.5	4.7	97.0
		5.0	4.8 ± 0.2	4.2	96.0
Noodle 2	ND	10.0	10.1 ± 0.3	2.8	101.0
		5.0	4.7 ± 0.2	4.1	94.0
Noodle 3	ND	10.0	10.3 ± 0.4	3.9	103.0

4. Conclusions

The sensing studies and applications of CsPbX₃ NCs in analytical chemistry mainly benefit from its excellent optical and photoelectric properties such as high quantum yield, narrow half-peak width, and ion exchange, which has excellent application prospects in colorimetric sensing. Through the ratio of halogen ions in CsPbX₃ NCs, the emission wavelength of their fluorescence spectra can be regulated to cover the whole visible region and produce significant color change from blue to red, which is very beneficial in colorimetric sensing with high visual sensitivity based on wavelength-shift. However, CsPbX₃ NCs are unstable in water due to their intrinsic ionic salt properties, low surface energy generation, and limited ion radius tolerance factor, which creates challenges for their application in an aqueous medium. In this study, we have discussed the halogen exchange Br[−] in CsPbBr₃ PNCs and I[−] in OLAM-I under three homogeneous phases: solid/liquid (organic phase), liquid (water phase)/liquid (organic phase), and liquid (organic phase)/liquid (organic phase). The experimental results show that Br[−] in CsPbBr₃ PNCs and I[−] in OLAM-I causes rapid halogen exchange, and results in a fluorescence emission wavelength shift. Based on these results, we have realized the feasibility of the colorimetric sensing of BPO, in which the reaction between OLAM-I and BPO caused a concentration change of OLAM-I. Using the halogen exchange, we have successfully developed an indirect approach for the colorimetric sensing of BPO with high visualization resolution, fast response, and high sensitivity, and attained the determination of BPO in flour and noodle samples. Based on this consideration, we can realize the discovery of other oxides in the organic system, such as hydrogen peroxide, or introduce a microemulsion system and enzymatic catalytic oxidation to achieve the colorimetric sensing in a biological system, which will further broaden the application of CsPbBr₃ PNCs in analytical sensing.

Supplementary Materials: The following are available online at <https://www.mdpi.com/article/10.3390/chemosensors9110319/s1>, Table S1: The sensing applications of perovskite material, Table S2: Comparison among the results from the present work and others found in the reference.

Author Contributions: Experiments, investigation, and original draft preparation, L.Z. (Li Zhang) and Y.Z.; methodology and visualization, F.L., L.Z. (Linchun Zhang) and Z.G.; review and editing, Y.H. and L.Y.; visualization, F.L.; project administration, L.Z. (Li Zhao); funding acquisition, supervision, and writing, X.C. All authors have read and agreed to the published version of the manuscript.

Funding: This research was funded by the National Natural Science Foundations of China, grant number 21876141, and the Shenzhen Science and Technology Project, grant number JCYJ20180306172823786.

Institutional Review Board Statement: Not applicable.

Informed Consent Statement: Not applicable.

Data Availability Statement: Data are contained within the article.

Conflicts of Interest: The authors declare no conflict of interest. The funders had no role in the design of the study; in the collection, analyses, or interpretation of data; in the writing of the manuscript; or in the decision to publish the results.

References

1. Møller, C.K.N. Crystal Structure and Photoconductivity of Caesium Plumbohalides. *Nat. Cell Biol.* **1958**, *182*, 1436. [[CrossRef](#)]
2. Kojima, A.; Teshima, K.; Shirai, Y.; Miyasaka, T. Organometal Halide Perovskites as Visible-Light Sensitizers for Photovoltaic Cells. *J. Am. Chem. Soc.* **2009**, *131*, 6050–6051. [[CrossRef](#)]
3. Lin, K.; Xing, J.; Quan, L.N.; de Arquer, F.P.G.; Gong, X.; Lu, J.; Xie, L.; Zhao, W.; Zhang, D.; Yan, C.; et al. Perovskite light-emitting diodes with external quantum efficiency exceeding 20 percent. *Nature* **2018**, *562*, 245–248. [[CrossRef](#)]
4. Chen, Q.; Wu, J.; Ou, X.; Huang, B.; Almutlaq, J.; Zhumekeenov, A.A.; Guan, X.; Han, S.; Liang, L.; Yi, Z.; et al. All-inorganic perovskite nanocrystal scintillators. *Nat. Cell Biol.* **2018**, *561*, 88–93. [[CrossRef](#)]
5. Zhang, Y.; Sun, R.; Ou, X.; Fu, K.; Chen, Q.; Ding, Y.; Xu, L.-J.; Liu, L.; Han, Y.; Malko, A.V.; et al. Metal Halide Perovskite Nanosheet for X-ray High-Resolution Scintillation Imaging Screens. *ACS Nano* **2019**, *13*, 2520–2525. [[CrossRef](#)] [[PubMed](#)]

6. Yakunin, S.; Chaaban, J.; Benin, B.M.; Cherniukh, I.; Bernasconi, C.; Landuyt, A.; Shynkarenko, Y.; Bolat, S.; Hofer, C.; Romanyuk, Y.E.; et al. Radiative lifetime-encoded unicolour security tags using perovskite nanocrystals. *Nature Comm.* **2021**, *12*, 981. [[CrossRef](#)] [[PubMed](#)]
7. Tong, Y.; Wang, Q.; Liu, X.; Mei, E.; Liang, X.; Xiang, W. The promotion of TiO₂ induction for finely tunable self-crystallized CsPbX₃ (X = Cl, Br and I) nanocrystal glasses for LED backlighting display. *Chem. Eng. J.* **2022**, *429*, 132391. [[CrossRef](#)]
8. Song, J.; Li, J.; Li, X.; Xu, L.; Dong, Y.; Zeng, H. Quantum Dot Light-Emitting Diodes Based on Inorganic Perovskite Cesium Lead Halides (CsPbX₃). *Adv. Mater.* **2015**, *27*, 7162–7167. [[CrossRef](#)]
9. Fu, Y.; Zhu, H.; Stoumpos, C.; Ding, Q.; Wang, J.; Kanatzidis, M.G.; Zhu, X.; Jin, S. Broad Wavelength Tunable Robust Lasing from Single-Crystal Nanowires of Cesium Lead Halide Perovskites (CsPbX₃, X = Cl, Br, I). *ACS Nano* **2016**, *10*, 7963–7972. [[CrossRef](#)] [[PubMed](#)]
10. Qin, C.; Sandanayaka, A.S.D.; Zhao, C.; Matsushima, T.; Zhang, D.; Fujihara, T.; Adachi, C. Stable room-temperature continuous-wave lasing in quasi-2D perovskite films. *Nat. Cell Biol.* **2020**, *585*, 53–57. [[CrossRef](#)]
11. Zhu, Y.; Li, F.; Huang, Y.; Lin, F.; Chen, X. Wavelength-Shift-Based Colorimetric Sensing for Peroxide Number of Edible Oil Using CsPbBr₃ Perovskite Nanocrystals. *Anal. Chem.* **2019**, *91*, 14183–14187. [[CrossRef](#)] [[PubMed](#)]
12. Zhu, Z.; Sun, Q.; Zhang, Z.; Dai, J.; Xing, G.; Li, S.; Huang, X.; Huang, W. Metal halide perovskites: Stability and sensing-ability. *J. Mater. Chem. C* **2018**, *6*, 10121–10137. [[CrossRef](#)]
13. Huang, S.; Guo, M.; Tan, J.; Geng, Y.; Wu, J.; Tang, Y.; Su, C.; Lin, C.C.; Liang, Y. Novel Fluorescence Sensor Based on All-Inorganic Perovskite Quantum Dots Coated with Molecularly Imprinted Polymers for Highly Selective and Sensitive Detection of Omethoate. *ACS Appl. Mater. Interfaces* **2018**, *10*, 39056–39063. [[CrossRef](#)]
14. Shamsi, J.; Urban, A.S.; Imran, M.; De Trizio, L.; Manna, L. Metal Halide Perovskite Nanocrystals: Synthesis, Post-Synthesis Modifications, and Their Optical Properties. *Chem. Rev.* **2019**, *119*, 3296–3348. [[CrossRef](#)]
15. Schmidt, L.; Pertegás, A.; Gonzalez-Carrero, S.; Malinkiewicz, O.; Agouram, S.; Espallargas, G.M.; Bolink, H.; Galian, R.E.; Pérez-Prieto, J. Nontemplate Synthesis of CH₃NH₃PbBr₃ Perovskite Nanoparticles. *J. Am. Chem. Soc.* **2014**, *136*, 850–853. [[CrossRef](#)]
16. Protesescu, L.; Yakunin, S.; Bodnarchuk, M.I.; Krieg, F.; Caputo, R.; Hendon, C.H.; Yang, R.X.; Walsh, A.; Kovalenko, M.V. Nanocrystals of Cesium Lead Halide Perovskites (CsPbX₃, X = Cl, Br, and I): Novel Optoelectronic Materials Showing Bright Emission with Wide Color Gamut. *Nano Lett.* **2015**, *15*, 3692–3696. [[CrossRef](#)] [[PubMed](#)]
17. Akkerman, Q.; D’Innocenzo, V.; Accornero, S.; Scarpellini, A.; Petrozza, A.; Prato, M.; Manna, L. Tuning the Optical Properties of Cesium Lead Halide Perovskite Nanocrystals by Anion Exchange Reactions. *J. Am. Chem. Soc.* **2015**, *137*, 10276–10281. [[CrossRef](#)] [[PubMed](#)]
18. Lu, L.-Q.; Tan, T.; Tian, X.-K.; Li, Y.; Deng, P. Visual and sensitive fluorescent sensing for ultratrace mercury ions by perovskite quantum dots. *Anal. Chim. Acta* **2017**, *986*, 109–114. [[CrossRef](#)] [[PubMed](#)]
19. Xu, W.; Li, F.; Cai, Z.; Wang, Y.; Luo, F.; Chen, X. An ultrasensitive and reversible fluorescence sensor of humidity using perovskite CH₃NH₃PbBr₃. *J. Mater. Chem. C* **2016**, *4*, 9651–9655. [[CrossRef](#)]
20. Chen, C.; Cai, Q.; Luo, F.; Dong, N.; Guo, L.; Qiu, B.; Lin, Z. Sensitive Fluorescent Sensor for Hydrogen Sulfide in Rat Brain Microdialysis via CsPbBr₃ Quantum Dots. *Anal. Chem.* **2019**, *91*, 15915–15921. [[CrossRef](#)]
21. Rodà, C.; Abdelhady, A.L.; Shamsi, J.; Lorenzon, M.; Pinchetti, V.; Gandini, M.; Meinardi, F.; Manna, L.; Brovelli, S. O₂ as a molecular probe for nonradiative surface defects in CsPbBr₃ perovskite nanostructures and single crystals. *Nanoscale* **2019**, *11*, 7613–7623. [[CrossRef](#)]
22. Lin, F.; Li, F.; Lai, Z.; Cai, Z.; Wang, Y.; Wolfbeis, O.S.; Chen, X. MnII-Doped Cesium Lead Chloride Perovskite Nanocrystals: Demonstration of Oxygen Sensing Capability Based on Luminescent Dopants and Host-Dopant Energy Transfer. *ACS Appl. Mater. Interfaces* **2018**, *10*, 23335–23343. [[CrossRef](#)]
23. Li, F.; Feng, Y.; Huang, Y.; Yao, Q.; Huang, G.; Zhu, Y.; Chen, X. Colorimetric sensing of chloride in sweat based on fluorescence wavelength shift via halide exchange of CsPbBr₃ perovskite nanocrystals. *Microchim. Acta* **2021**, *188*, 1–8. [[CrossRef](#)]
24. Huang, Y.; Wang, S.; Zhu, Y.; Li, F.; Jin, J.; Dong, J.; Lin, F.; Wang, Y.; Chen, X. Dual-Mode of Fluorescence Turn-On and Wavelength-Shift for Methylamine Gas Sensing Based on Space-Confined Growth of Methylammonium Lead Tribromide Perovskite Nanocrystals. *Anal. Chem.* **2020**, *92*, 5661–5665. [[CrossRef](#)]
25. Yin, W.; Li, H.; Chesman, A.S.R.; Tadjell, B.; Scully, A.D.; Wang, M.; Huang, W.; McNeill, C.R.; Wong, W.W.H.; Medhekar, N.V.; et al. Detection of Halomethanes Using Cesium Lead Halide Perovskite Nanocrystals. *ACS Nano* **2021**, *15*, 1454–1464. [[CrossRef](#)] [[PubMed](#)]
26. Park, B.; Kang, S.-M.; Lee, G.W.; Kwak, C.H.; Rethinasabapathy, M.; Huh, Y.S. Fabrication of CsPbBr₃ Perovskite Quantum Dots/Cellulose-Based Colorimetric Sensor: Dual-Responsive On-Site Detection of Chloride and Iodide Ions. *Ind. Eng. Chem. Res.* **2019**, *59*, 793–801. [[CrossRef](#)]
27. Ministry of Health; Ministry of Industry and Information Technology; Ministry of Commerce; The State Administration of Industry and Commerce; General Administration of Quality Supervision; State Grain Administration; State Food and Drug Administration. *Announcement of Ministry of Health and Other Seven Departments on Revoking Benzoyl Peroxide and Calcium Peroxide as Food Additives*; Chinese Journal of Food Hygiene: Beijing, China, 2011.
28. Zhang, S. Detection of benzoyl peroxide in food by gas chromatography. *J. Food Saf. Qual.* **2016**, *7*, 353–356.

29. The General Administration of Quality Supervision; Inspection and Quarantine of the People's Republic of China; The Standardization Administration of China. *Determination of Benzoyl Peroxide in Wheat Flour by High Performance Liquid Chromatography (GB/T 22325-2008)*; Standards Press of China: Beijing, China, 2008.
30. Saiz, A.I.; Manrique, G.D.; Fritz, R. Determination of benzoyl peroxide and benzoic acid levels by HPLC during wheat flour bleaching process. *J. Agric. Food Chem.* **2001**, *49*, 98–102. [[CrossRef](#)] [[PubMed](#)]
31. Abe-Onishi, Y.; Yomota, C.; Sugimoto, N.; Kubota, H.; Tanamoto, K. Determination of benzoyl peroxide and benzoic acid in wheat flour by high-performance liquid chromatography and its identification by high-performance liquid chromatography–mass spectrometry. *J. Chromatogr. A* **2004**, *1040*, 209–214. [[CrossRef](#)]
32. Mu, G.; Liu, H.; Gao, Y.; Luan, F. Determination of benzoyl peroxide, as benzoic acid, in wheat flour by capillary electrophoresis compared with HPLC. *J. Sci. Food Agric.* **2011**, *92*, 960–964. [[CrossRef](#)] [[PubMed](#)]
33. Kozan, J.; Silva, R.; Serrano, S.; Lima, A.; Angnes, L. Amperometric detection of benzoyl peroxide in pharmaceutical preparations using carbon paste electrodes with peroxidases naturally immobilized on coconut fibers. *Biosens. Bioelectron.* **2010**, *25*, 1143–1148. [[CrossRef](#)]
34. Wang, C.; Hu, X. Determination of Benzoyl Peroxide Levels in Wheat Flour and Pharmaceutical Preparations by Differential Pulse Voltammetry in Nonaqueous Media. *Anal. Lett.* **2005**, *38*, 2175–2187. [[CrossRef](#)]
35. Bowyer, J.; Spurlin, S. Chemiluminescence method for determination of benzoyl peroxide in solution. *Anal. Chim. Acta* **1987**, *192*, 289–292. [[CrossRef](#)]
36. Yang, W.-P.; Zhang, Z.-J.; Hun, X. A novel capillary microliter droplet sample injection–chemiluminescence detector and its application to the determination of benzoyl peroxide in wheat flour. *Talanta* **2003**, *62*, 661–666. [[CrossRef](#)]
37. Wang, S.P.; Liu, X. The clinical features, CT and MRI diagnosis of Wallenberg syndrome. *J. Taishan. Med. Colle.* **2010**, *31*, 446–447.
38. Hu, Q.; Li, W.; Qin, C.; Zeng, L.; Hou, J.-T. Rapid and Visual Detection of Benzoyl Peroxide in Food by a Colorimetric and Ratiometric Fluorescent Probe. *J. Agric. Food Chem.* **2018**, *66*, 10913–10920. [[CrossRef](#)]
39. Zeng, L.; Wu, X.; Hu, Q.; Yuan, H.-Q.; Bao, G.-M. A single fluorescent chemosensor for discriminative detection of bisulfite and benzoyl peroxide in food with different emission. *Sensors Actuators B Chem.* **2019**, *299*, 126994. [[CrossRef](#)]
40. Wu, X.; Zeng, L.; Chen, B.-Q.; Zhang, M.; Rodrigues, J.; Sheng, R.; Bao, G.-M. A selective cascade reaction-based probe for colorimetric and ratiometric fluorescence detection of benzoyl peroxide in food and living cells. *J. Mater. Chem. B* **2019**, *7*, 5775–5781. [[CrossRef](#)] [[PubMed](#)]
41. Lin, T.; Zhang, M.; Xu, F.; Wang, X.; Xu, Z.; Guo, L. Colorimetric detection of benzoyl peroxide based on the etching of silver nanoshells of Au@Ag nanorods. *Sensors Actuators B Chem.* **2018**, *261*, 379–384. [[CrossRef](#)]
42. Akkerman, Q.A.; Martínez-Sarti, L.; Goldoni, L.; Imran, M.; Baranov, D.; Bolink, H.J.; Palazon, F.; Manna, L. Molecular Iodine for a General Synthesis of Binary and Ternary Inorganic and Hybrid Organic–Inorganic Iodide Nanocrystals. *Chem. Mater.* **2018**, *30*, 6915–6921. [[CrossRef](#)]
43. Hoffman, J.B.; Schleper, A.L.; Kamat, P.V. Transformation of Sintered CsPbBr₃ Nanocrystals to Cubic CsPbI₃ and Gradient CsPbBr_xI_{3-x} through Halide Exchange. *J. Am. Chem. Soc.* **2016**, *138*, 8603–8611. [[CrossRef](#)] [[PubMed](#)]